



Cancer Research

Tpx2 Controls Spindle Integrity, Genome Stability, and Tumor Development

Cristina Aguirre-Portolés, Alexander W. Bird, Anthony Hyman, et al.

Cancer Res 2012;72:1518-1528. Published OnlineFirst January 20, 2012.

Updated Version

Access the most recent version of this article at:
doi:[10.1158/0008-5472.CAN-11-1971](https://doi.org/10.1158/0008-5472.CAN-11-1971)

Supplementary Material

Access the most recent supplemental material at:
<http://cancerres.aacrjournals.org/content/suppl/2012/01/20/0008-5472.CAN-11-1971.DC1.html>

Cited Articles

This article cites 43 articles, 14 of which you can access for free at:
<http://cancerres.aacrjournals.org/content/72/6/1518.full.html#ref-list-1>

E-mail alerts

[Sign up to receive free email-alerts](#) related to this article or journal.

Reprints and Subscriptions

To order reprints of this article or to subscribe to the journal, contact the AACR Publications Department at pubs@aacr.org.

Permissions

To request permission to re-use all or part of this article, contact the AACR Publications Department at permissions@aacr.org.

Tpx2 Controls Spindle Integrity, Genome Stability, and Tumor Development

Cristina Aguirre-Portolés¹, Alexander W. Bird³, Anthony Hyman³, Marta Cañamero², Ignacio Pérez de Castro¹, and Marcos Malumbres¹

Abstract

Tpx2 is a microtubule-associated protein that activates the cell-cycle kinase Aurora A and regulates the mitotic spindle. Overexpression of Tpx2 is associated with the development of different human tumors and strongly correlates with chromosomal instability. By analyzing a conditional null mutation in the mouse *Tpx2* gene, we show here that Tpx2 expression is essential for spindle function and chromosome segregation in the mouse embryo. Conditional genetic ablation of Tpx2 in primary cultures resulted in deficient microtubule nucleation from DNA and aberrant spindles during prometaphase. These cells eventually exited from mitosis without chromosome segregation. In addition, Tpx2 haploinsufficiency led to the accumulation of aneuploidies *in vivo* and increased susceptibility to spontaneous lymphomas and lung tumors. Together, our findings indicate that Tpx2 is essential for maintaining genomic stability through its role in spindle regulation. Subtle changes in Tpx2 expression may favor tumor development *in vivo*. *Cancer Res*; 72(6); 1518–28. ©2012 AACR.

Introduction

Formation of a proper bipolar spindle is an essential process required for accurate chromosome segregation. This dynamic microtubule-based structure is responsible for chromosomal movements that ensure the equal distribution of a single, complete complement of the genome into 2 daughter cells. Chromatin-driven microtubule nucleation and organization depends on a gradient of Ran-GTP known to promote microtubule nucleation and stabilization surrounding the chromosomes (1). Tpx2 is one of the best studied factors regulated by the Ran-GTP gradient during mitosis. First described by Wittmann and colleagues in 1998 as the Targeting Protein for Xklp2 in *Xenopus laevis* (2), this protein regulates the spindle formation at different levels. Once released from its inhibitory complex with importin- α , Tpx2 is able to promote microtubule nucleation from the chromatin, both in *Xenopus* extracts and in human cells (3–5). Tpx2 recruits Aurora A kinase to microtubules (6) and drives the activation of this kinase during mitosis (7, 8). The N-terminal domain of Tpx2 interacts with Aurora A protecting the Thr288 in the T-loop of the kinase from

dephosphorylation by the Phosphatase Protein 1 (PP1; refs. 7, 9). Cells deficient in the Aurora A/Tpx2 complex present short spindles which, despite of being able to segregate chromosomes, result in mitotic failure (4).

Alterations in the expression levels of several mitotic regulators have been associated with tumor formation in humans (reviewed in refs. 10, 11). In fact, either upregulation or downregulation of several mitotic regulators may lead to spontaneous tumor formation through an increase in aneuploidy (11, 12). For instance, both downregulation and overexpression of Mad2 (also called MAD2L1) result in increased susceptibility to tumor development (13, 14). Aurora A is also overexpressed in various cancers including breast, colorectal, and bladder tumors (10), and its partial deficiency results in pulmonary carcinomas, squamous cell carcinoma, and lymphomas in Aurora A heterozygous mice (15). Tpx2 is also highly expressed in human tumors (reviewed in refs. 10, 16) and overexpression of Tpx2 displays the highest correlation with the presence of chromosomal instability (CIN) in several human cancers (17).

To understand the physiologic relevance of Tpx2, we have generated Tpx2-deficient embryos and mice. Complete genetic ablation of Tpx2 results in defective microtubule nucleation and spindle abnormalities that prevent chromosome segregation in early embryos or cultured fibroblasts. Partial deficiency in Tpx2 levels results in the accumulation of aneuploidy *in vitro* and *in vivo* and shorter lifespan due to spontaneous tumor development, suggesting that the control of spindle integrity by Tpx2 prevents genomic instability *in vivo*.

Materials and Methods

Generation and characterization of Tpx2 mutant mice

The ES cell clone D028B03 was obtained from the Gene Trap German Consortium (GGTC). The exact position of the

Authors' Affiliations: ¹Cell Division and Cancer Group, Spanish National Cancer Research Center (CNIO); ²Comparative Pathology Unit, Centro Nacional de Investigaciones Oncológicas (CNIO), Madrid, Spain; and ³Department of Microtubules and Cell Division, Max Planck Institute of Molecular Cell Biology and Genetics, Dresden, Germany

Note: Supplementary data for this article are available at Cancer Research Online (<http://cancerres.aacrjournals.org/>).

Corresponding Authors: Ignacio Pérez de Castro, Centro Nacional de Investigaciones Oncológicas (CNIO), Melchor Fernández Almagro 3, E-28029 Madrid. Phone: 34-91-732-8000; Fax: 34-91-732-8033; E-mail: iperez@cnio.es; and Marcos Malumbres, E-mail: malumbres@cnio.es

doi: 10.1158/0008-5472.CAN-11-1971

©2012 American Association for Cancer Research.

insertion was determined by PCR and DNA sequencing (Fig. 1). Chimeras were generated through standard blastocyst microinjection. *Tpx2* heterozygous mice were obtained by intercrossing with C57BL/6J wild-type mice. Genotyping of *Tpx2* alleles (wild type, trapped allele, conditional, and knockout) was done by PCR using the following oligonucleotides: wild-type allele (+): *Tpx2*_D028B03_F2: 5'-GAA-TTCAGAGGCCAGACAG-3'; *Tpx2*_D028B03_R2: 5'-GAGTTCAGGACAGCCAGAG-3'; trapped allele (-): *Tpx2*_D028B03_F2: 5'-GAATTCAGAGGCCAGACAG-3'; *Tpx2*_D028B03_R1: 5'-CTCCGAAAACCGCTTCTA-3; conditional allele (lox): *Tpx2*_D028B03_F3: 5'-TTCTCTGCATAGCCCAAGGT-3; *Tpx2*_D028B03_R3: 5'-GGGAGATTGGGAAGACAAT-3; knockout allele (Δ): *Tpx2*_D028B03_F3: 5'-TTCTCTGCATAGCCCAAGGT -3' B32: 5'-CAAGGCGATTAAGTTGGGTAACG-3'.

Mice were housed at the pathogen-free animal facility of the Centro Nacional de Investigaciones Oncológicas (Madrid)

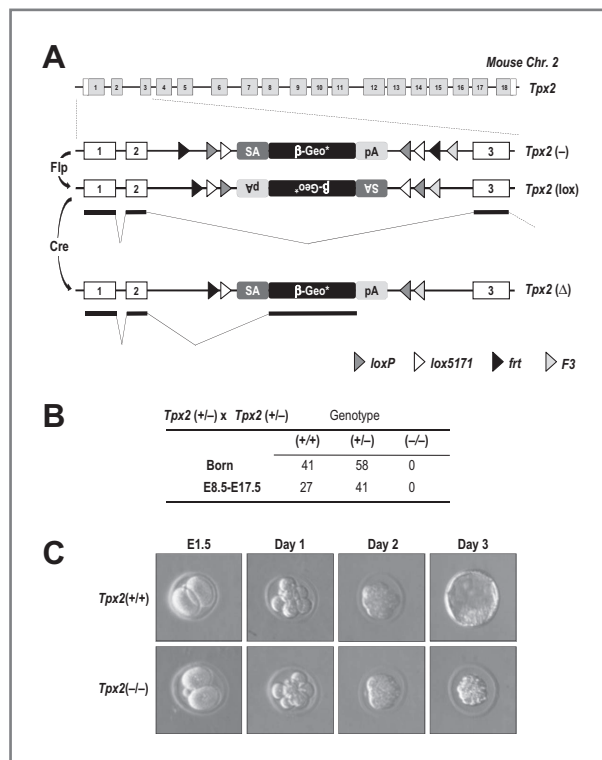


Figure 1. Early embryonic lethality in the absence of *Tpx2*. **A**, wild-type and mutant *Tpx2* alleles used in this study are represented. *Tpx2* trapped allele (-) is the result of the insertion of a β -geo resistance cassette in intron 2, abrogating *Tpx2* protein expression through the recognition of the splicing acceptor (SA). This cassette is flanked by wild-type and mutant (F3) frt sites (black and light grey triangles), loxP sites (dark grey triangles), lox5171 (white triangles). Flp recombinase recognizes frt sites, resulting in an inversion of the cassette (21) and generating the *Tpx2* conditional allele (*Tpx2*^{lox}). Cre induces a new inversion through the recombination of loxP and lox5171 sites generating the knockout allele (*Tpx2* ^{Δ}). SA, splicing acceptor; pA, poly (A) tail. **B**, observed number of genotyped pups or embryos from *Tpx2*^{+/-} intercrosses. **C**, *ex vivo* culture of embryos from *Tpx2*^{+/-} intercrosses. Embryos were extracted at embryonic day (E)1.5 and maintained in culture for 3 additional days.

following the animal care standards of the institution. These animals were observed daily and sick mice were euthanized humanely in accordance with the Guidelines for Humane End Points for Animals used in biomedical research. For histologic studies, dissected organs were fixed in 10% buffered formalin (Sigma) and embedded in paraffin wax. Sections of 3- or 5- μ m thickness were stained with hematoxylin and eosin (H&E).

Early embryo culture and immunofluorescence

Fertilized embryos were collected by flushing the oviduct through the infundibulum of super-ovulated females from crosses between *Tpx2*^{+/-} mice, with HEPES-buffered Medium 2 (M2; Sigma) at embryonic day (E)1.5. Embryos were individually cultured *in vitro* in potassium simplex optimized medium (KSOM; Chemicon International Inc.) and photographed daily for up to 4 days. PCR analysis of embryos was done as described previously (18). For immunofluorescence analysis, embryos were fixed with cold methanol during 1 hour at -20°C, washed in PBS containing 0.1% bovine serum albumin (BSA; Sigma) and incubated with 0.1% Triton X-100. Embryos were then blocked with 10% of serum in PBS-0.1% BSA and incubated with the following primary antibodies: α -tubulin (mouse monoclonal, clone DM1a, 1:2,000; Sigma), Anti-Centromere Antibody (ACA, 1:100; Antibodies Inc.), and *Tpx2* (Rabbit polyclonal, 1:200, Lifespan) for 2 hours at 37°C. The matching secondary antibodies, with different Alexa dyes (488, 594, and 647, 1:1,000), are from Molecular Probes (1:250; Invitrogen). Images were obtained using a confocal ultraspectral microscope (Leica TCS-SP2-AOBS-UV) or confocal ultraspectral microscope Leica TCS-SP5).

Mouse embryonic fibroblast culture, immunofluorescence, and cytometry

Mouse embryonic fibroblasts (MEF) were generated from E13.5 embryos and cultured using standard protocols (19). Adenoviruses expressing Flp or Cre (supplied by the Iowa University) and siRNAs against *Mad2* (Dharmacon) were used following the manufacturer's recommendations. Briefly, adenoviruses were transduced in confluence and low serum conditions and, 48 hours later, cells were split and nucleofected with the corresponding siRNA. For immunofluorescence, cells were rinsed with PBS and fixed in 4% PFA-PBS for 7 minutes and then left in cold methanol overnight at -20°C. Cells were stained with antibodies against α -tubulin (mouse monoclonal, clone DM1a, 1:1,000; Sigma), CREST (1:500; A. Hyman's lab), Eg5 (kindly provided by Dr. Yannick Arlot-Bonnemains; rabbit polyclonal 1:250), Kif15 (kindly provided by Isabelle Vernos; rabbit polyclonal 1:250), *Tpx2* (rabbit polyclonal, 1:500, Lifespan; or rabbit polyclonal from A. Hyman's lab; 1:500), Cep135 (1:500, A. Hyman's lab), γ -tubulin (mouse monoclonal, clone GTU88, 1:1,000; Sigma), or Aurora A (mouse monoclonal, clone 35C1, 1:500; Abcam) for 1 hour at room temperature. Secondary antibodies (Alexa 488, 594, or 647; 1:1,000) were incubated for 1 hour at room temperature. Images were taken using a Leica D3000 microscope or confocal ultraspectral microscope Leica TCS-SP5. For DNA content analysis, cells were fixed in 70% ethanol overnight

at -20°C and stained with propidium iodide (20 $\mu\text{g}/\text{mL}$; Sigma) in presence of RNase A (0.2 mg/mL ; Qiagen) for 30 minutes at 4°C and then analyzed by flow cytometry (Becton-Dickinson).

Biochemical analysis and reverse transcriptase PCR

For immunoblotting, cells were harvested and lysed with radioimmunoprecipitation assay buffer and 50 μg of total protein was separated by SDS-PAGE and probed with antibodies against Tpx2 (rabbit polyclonal, 1:500, A. Hyman's lab), Mad2 (Mouse monoclonal, 1:500, MBL International) or β -actin (mouse monoclonal 1:2,000; Abcam). For quantitative reverse transcriptase PCR (RT-PCR), TRI Reagent (Invitrogen) and the SuperScript III Platinum One-Step qRT-PCR Kit were used as recommended by the manufacturers. The sequence of the specific primers used for Tpx2 is available under request to the authors.

Time-lapse imaging and microtubule growth assays

MEFs were transduced with a lentiviral vector expressing H2B protein fused to mRFP (pHIV-H2BmRFP; ref. 20). Fourteen hours after serum stimulation (15% FBS) of quiescent cells, time-lapse images were acquired using a DeltaVision RT imaging system (Applied Precision, LLC; IX70/71; Olympus) equipped with a charge-coupled device camera (CoolSNAP HQ; Roper Scientific). Images were acquired at 10 minutes intervals using a 20X PlanApo N 1.42 N.A. lens. Video analysis was carried out with LAS-AF Lite software (Leica). Microtubule regrowth assays were done using $Tpx2^{\text{lox/lox}}$ and $Tpx2^{\Delta/\Delta}$ MEFs treated with 100 ng/mL nocodazole for 6 hours to increase percentage of cells in M phase. Cells were incubated with 15% FBS during 24 hours after serum addition. Samples were then transferred to ice-cold media supplemented with 10 mmol/L HEPES, pH 7.25, for 40 minutes to fully depolymerize microtubules. Cells were then transferred to the same medium at 37°C for 3 or 10 minutes to allow microtubule regrowth and fixed immediately in cold methanol. For cold-stable microtubule assays, 28 hours after serum addition cells were transferred to ice-cold media for 5 minutes and fixed with 4% formaldehyde. Fixed images were acquired in 0.2- μm serial Z sections using a 100×1.35 NA UPLanApo objective in the DeltaVision equipment. Datasets were deconvolved using SoftWoRx (Applied Precision, LLC) software.

Metaphase spreads

Cells were hypotonically swollen in 40% full medium, 60% tap water for 5.5 minutes. Hypotonic treatment was stopped by adding an equal volume of Carnoy's solution (75% pure methanol, 25% glacial acetic acid), cells were then spun down, and resuspended and fixed with Carnoy's solution for 10 minutes. After fixation, cells were dropped from a 5-cm height onto glass slides previously treated with 45% of acetic acid. Slides were mounted with ProLong Gold anti-fade reagent with 4',6-diamidino-2-phenylindole (DAPI; Invitrogen) and images were acquired with a Leica D3000 microscope and a 60X PlanApo N 1.42 N.A. objective. Chromosomes from 30 cells per genotype were counted using ImageJ software.

Results

Tpx2 is required for cell division during early embryonic development

To study the physiologic functions of Tpx2 *in vivo* we used a conditional gene trap allele as represented in Fig. 1A (see Methods). This strategy consists on the insertion of a β -geo (β -galactosidase plus neo resistance) cassette that carries a splicing acceptor (SA) and a poly(A) sequence for termination of transcription. Alternated and inverted wild-type or mutant *frt* and *loxP* sites flanking the resistance cassette allow its inversion in the presence of Flp or Cre recombinases (21), allowing the switching from a conditional allele $Tpx2(\text{lox})$ to the null allele $Tpx2(\Delta)$, in which the $Tpx2$ transcript is trapped by the SA- β -geo cassette (Fig. 1A). Both the $Tpx2(-)$ and the $Tpx2(\Delta)$ are null alleles and led to similar phenotypes in homozygosity.

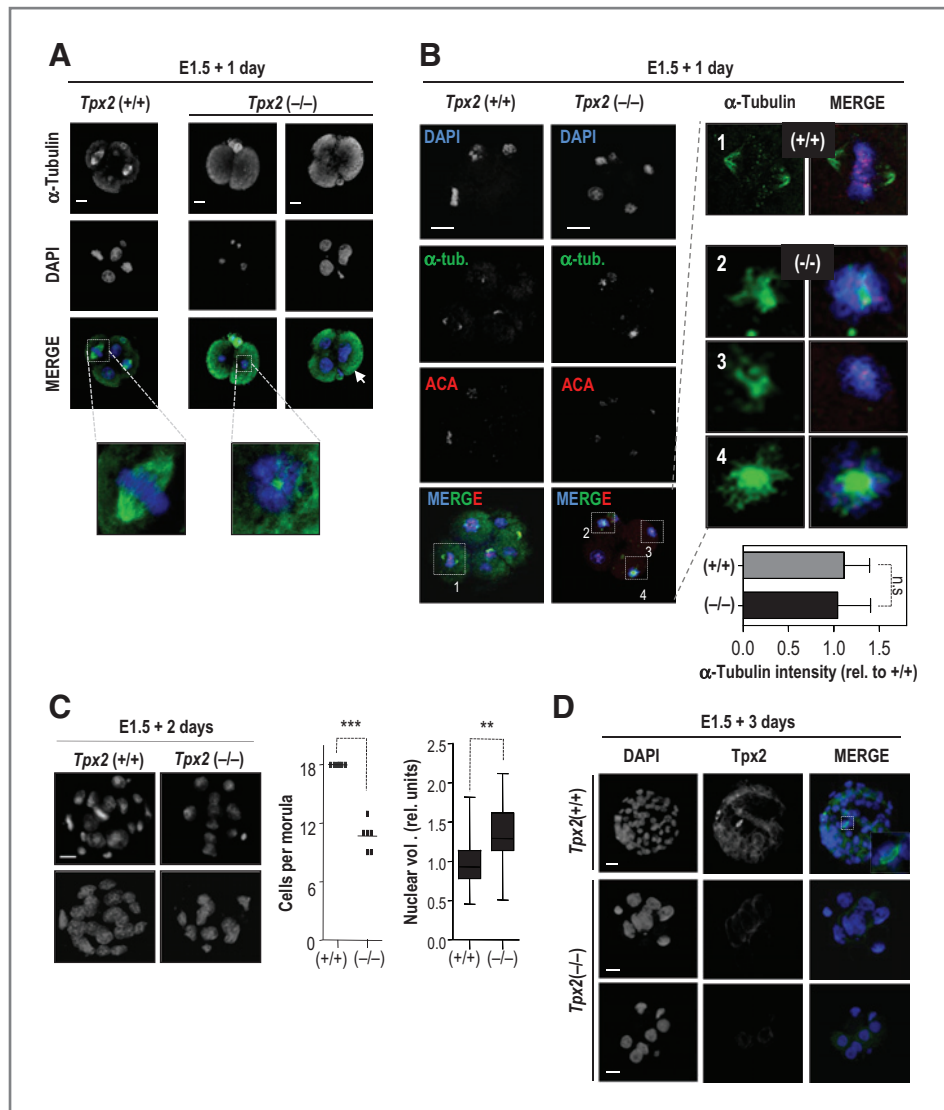
No homozygous $Tpx2^{-/-}$ mutant was born from intercrosses between $Tpx2^{+/-}$ mice and, similarly, null embryos were absent between embryonic day (E)8.5 and E17.5 (Fig. 1B), suggesting early embryonic lethality in the absence of Tpx2. We then harvested embryos at E1.5 and kept them in culture following its development by bright field microscopy. E1.5 $Tpx2^{-/-}$ embryos were observed at the expected Mendelian ratio (23%; $N = 97$). However, whereas $Tpx2^{+/+}$ and $Tpx2^{+/-}$ embryos were capable of generating normal blastocysts, Tpx2 null embryos got arrested at the morula stage (Fig. 1C), suggesting that Tpx2 is essential for preimplantational development of the mouse.

To characterize the origin of the early lethality, we carried out immunofluorescence 1 (early morula), 2 (compacted morula), or 3 (blastocyst) days after extracting the embryos at E1.5. Tpx2 null cells were not able to establish a proper bipolar spindle in early morulas and these cells presented collapsed or monopolar spindles (Fig. 2A and B). At this stage, we observed the presence of tetraploid cells that suggested defective chromosome segregation (Fig. 2A). Although the structure of the spindle was disturbed, no differences in the intensity of α -tubulin were observed when comparing wild-type bipolar spindles with the aberrant spindles observed in $Tpx2^{-/-}$ cells ($P = 0.8882$; Fig. 2B). After 2 days in culture, wild-type embryos presented 18 cells per morula, whereas the number of cells in mutant embryos varied from 9 to 13 ($P < 0.0001$; Fig. 2C). Tpx2 null cells presented a statistically significant increase in the volume of the nuclei ($P < 0.002$; Fig. 2C), suggesting lack of proper cell division. After 3 days in culture, $Tpx2^{-/-}$ embryos remained arrested at the morula stage, whereas wild-type embryos had formed early blastocysts and presented normal bipolar spindles in mitotic cells (Fig. 2D). These results indicated that Tpx2 is required for the formation of normal bipolar spindles and chromosome segregation during early embryonic development.

Defective cell-cycle progression and chromosome segregation in Tpx2 null MEFs

We took advantage of the possibility to abrogate the expression of Tpx2 in a conditional manner under Cre recombinase expression (Fig. 1A). We derived $Tpx2^{\text{lox/lox}}$ MEFs from E13.5

Figure 2. Lack of Tpx2 induces spindle defects during early embryo development. **A**, fluorescence microscopy analysis of E1.5 *Tpx2*^{+/+} and *Tpx2*^{-/-} embryos after 1 additional day in culture. Antibodies against α -tubulin (green) were used to mark microtubules. DAPI was used to stain DNA. Mitotic cells were identifiable by DNA condensation and α -tubulin staining. Note the spindle aberrancies displayed by *Tpx2*^{-/-} cells including a binucleated cell (arrow). Scale bar, 20 μ m. **B**, antibodies against α -tubulin and ACA were used to stain microtubules and centromeres, respectively, in E1.5 embryos after one additional day in culture. Individual cells are shown in the right panels. Note the spindle aberrancies displayed by *Tpx2*^{-/-} cells. No differences in α -tubulin intensity were found between *Tpx2*^{+/+} and *Tpx2*^{-/-} embryos ($P = 0.8882$). **C**, immunofluorescence of E1.5 *Tpx2*^{+/+} and *Tpx2*^{-/-} embryos after 2 additional days in culture. Differences in the number of cells (***, $P < 0.0001$) and nuclear volume (**, $P < 0.01$) were determined by DAPI staining. **D**, immunofluorescence of E1.5 *Tpx2*^{+/+} and *Tpx2*^{-/-} embryos after 3 additional days in culture. *Tpx2*^{+/+} embryos form blastocysts whereas *Tpx2*^{-/-} embryos remain arrested at morula stage with giant nuclei. Tpx2 is shown in green and DAPI (DNA) in blue. All scale bars, 20 μ m.



embryos and these cells were transduced with Cre expressing adenoviruses to genetically abrogate the expression of Tpx2 (*Tpx2* ^{Δ/Δ}). Flp recombinase was used as a control with no effect in *Tpx2*^{lox/lox} alleles. *Tpx2* ^{Δ/Δ} cultures showed a severe impairment in their proliferation capacity when compared with control MEFs ($P = 0.0026$; Fig. 3A). We then induced the genetic ablation of Tpx2 in serum-starved cells and followed cell-cycle progression by different techniques after the addition of serum (Fig. 3B). Control cells completed a normal cell cycle in about 28 hours, whereas Tpx2 null cells accumulated as 4N cells 28 or 32 hours after entering into the cell cycle. We also detected an increase in the percentage of *Tpx2* ^{Δ/Δ} cells with more than 4N DNA content (13.0% in *Tpx2* ^{Δ/Δ} vs. 7.5% in *Tpx2*^{lox/lox} at 24 hours; $P = 0.0061$; Fig. 3B). In addition, we observed a statistically significant increase in the sub-G₀ (less than 2N) population in Tpx2-deficient MEFs suggesting cell death in this population (Fig. 3B). Tpx2-deficient cultures also contained binucleated cells (Fig. 3C) as well as aberrant cells with multiple nuclei or micronuclei (Fig. 3C

and D). All these phenotypes suggested abnormal chromosome segregation and the presence of aberrant ploidy in Tpx2 null cells.

We next studied the onset and exit from mitosis following individual, synchronized cells in a time-lapse imaging experiment. To visualize chromatin, cells were transduced with a construct expressing histone H2B fused to mRFP (red fluorescence). The percentage of cells entering in mitosis was similar in *Tpx2*^{lox/lox} ($26.2 \pm 7.0\%$) and *Tpx2* ^{Δ/Δ} ($22.4 \pm 6.8\%$) MEFs ($P = 0.7315$; Fig. 4A). Control *Tpx2*^{lox/lox} MEFs were able to carry out mitosis in an average time of 73 minutes (73.1 ± 3.2 ; $N = 52$; Fig. 4B). In contrast, *Tpx2* ^{Δ/Δ} cells stayed in mitosis for an average time of 122 minutes (121.5 ± 12.4 ; $N = 39$) and exited mitosis without chromosome segregation and as a single cell in most cases (96.9%; Fig. 4A). A significant number of cells died in mitosis or during interphase after the first mitosis in agreement with the increase in the sub-G₀ population observed in previous assays (Fig. 3B). *Tpx2*^{+/-} cells presented no alteration in cell proliferation, mitotic progression, or nuclear

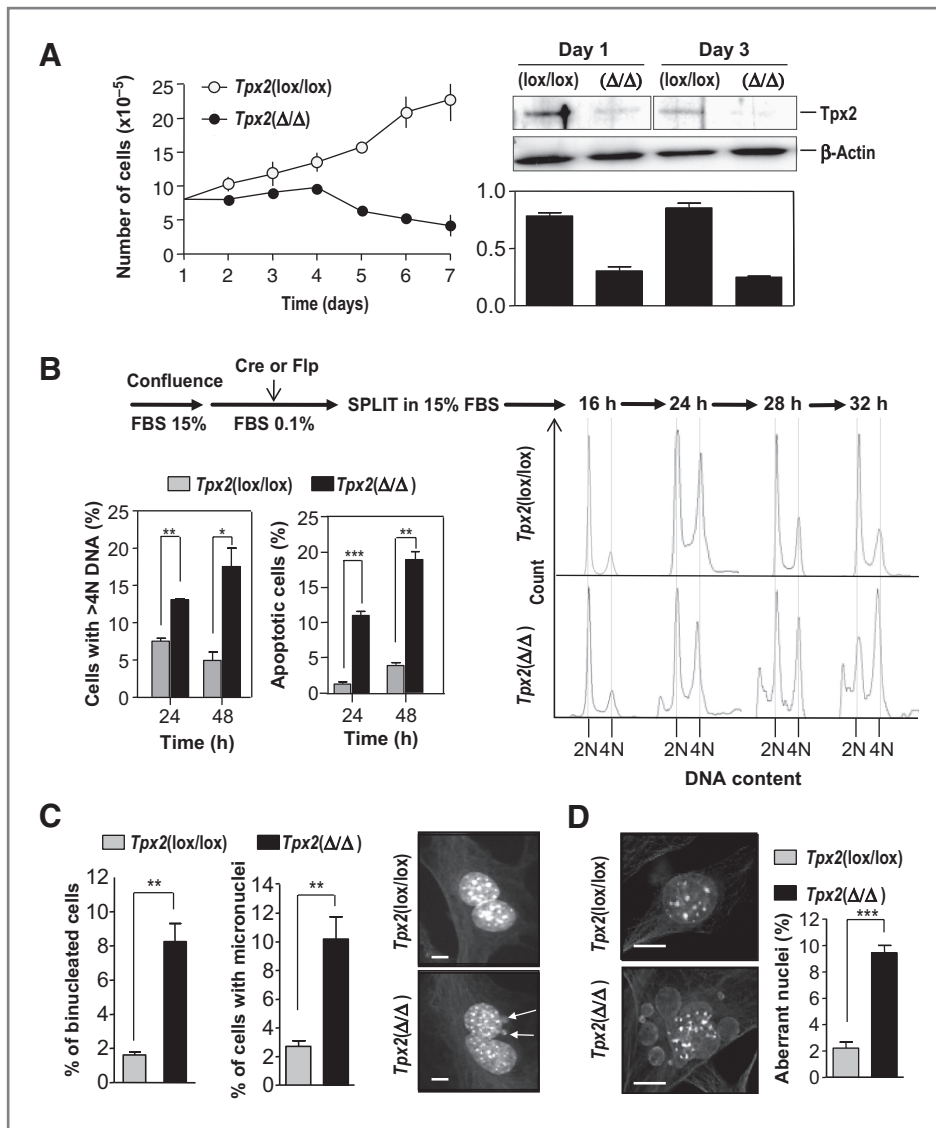


Figure 3. Proliferative defects in *Tpx2* null MEFs. **A**, growth of *Tpx2*^{lox/lox} or *Tpx2* ^{Δ/Δ} primary MEFs. Data were normalized against the number of cells seeded at day 1 and the experiment was carried out in triplicate ($P = 0.0026$). The ablation of *Tpx2* was confirmed by Western blot. **B**, experimental procedure to abrogate the expression of *Tpx2* in quiescent cells and to analyze the first cell cycle after *Tpx2* ablation. *Tpx2* ^{Δ/Δ} accumulate as 4N or more than 4N cells as detected by fluorescence-activated cell sorting for DNA content with propidium iodide. Left histogram shows the percentage of cells with more than 4N DNA content for each time point. Right histogram represents the percentage of apoptotic cells as determined by propidium iodide staining (less than 2N population). **C**, nuclear volume in *Tpx2*^{lox/lox} and *Tpx2* ^{Δ/Δ} MEFs 72 hours after stimulation with serum (scored after DAPI staining). Scale bar, 100 μ m. **D**, increased percentage of binucleated cells or cells with micronuclei in *Tpx2* ^{Δ/Δ} cultures. α -Tubulin, cytoplasmic signal, and DAPI, nuclear signal, are used in the representative micrographs. Scale bar, 10 μ m. **E**, increased percentage of multinucleated and polylobed nuclei in *Tpx2* ^{Δ/Δ} cultures (***, $P < 0.0001$; **, $P < 0.01$; *, $P < 0.05$). α -Tubulin, cytoplasmic signal; DAPI, nuclear signal. Scale bar, 10 μ m.

morphology when compared with wild-type cultures (Supplementary Fig. S1).

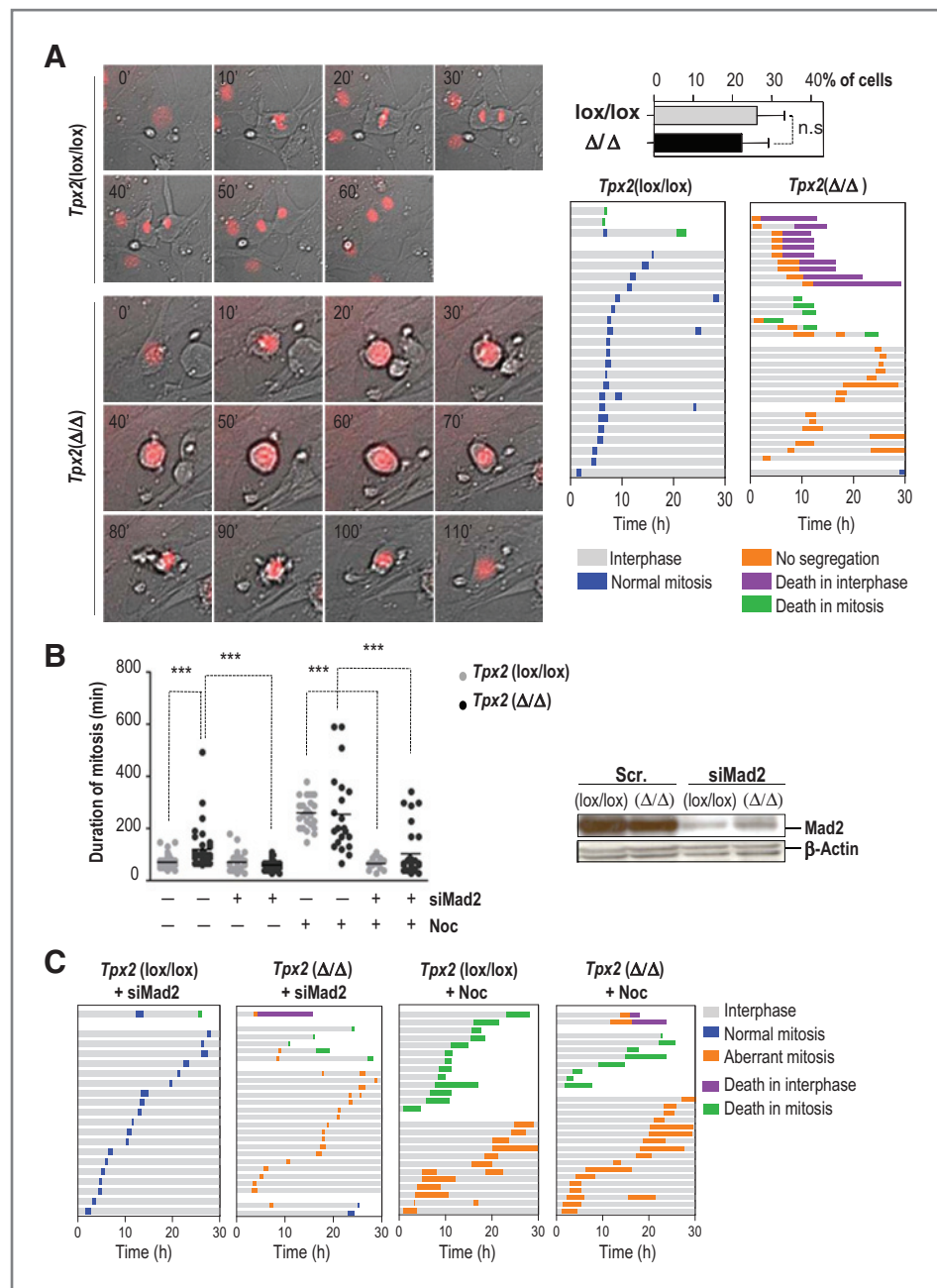
The spindle assembly checkpoint (SAC) is the main mechanism that delays mitotic exit until all chromosomes are bioriented in the presence of a normal spindle (for review, see ref. 22). Mad2 is required for monitoring proper chromosome attachment to the spindle microtubules during cell division, and the mitotic delay in presence of microtubule poisons can be overcome by depleting Mad2 from cells (Fig. 4B and C). Similarly, mitotic delay in *Tpx2* ^{Δ/Δ} cells was rescued in the presence of siRNAs against Mad2 (siMad2), and these cells quickly exited mitosis without chromosome segregation [duration of mitosis = 121.5 ± 12.37 minutes in *Tpx2* ^{Δ/Δ} ($N = 39$) vs. 61.61 ± 3.625 minutes in *Tpx2* ^{Δ/Δ} + siMad2 ($N = 31$); $P < 0.001$; Fig. 4B and C]. Cyclin B and securin are normally degraded during mitotic exit in *Tpx2* null cells and these mutant cells also display a slow but consistent degradation of cyclin B and securin in the presence of nocodazole (mitotic

slippage; data not shown). These data suggested that a SAC-dependent mechanism delays mitotic exit in *Tpx2* null cells, probably as a consequence of defects in the proper attachment of chromosomes to the abnormal spindle (see below) in the absence of *Tpx2*.

Tpx2 is essential for chromatin-dependent microtubule nucleation

Tpx2 null cells displayed a significant ($P < 0.001$) increase in prometaphase figures and the subsequent reduction in the number of metaphase, anaphase, or telophase figures (Fig. 5A), in agreement with the SAC-dependent delay reported above. This prometaphase arrest was associated with a range of spindle abnormalities that could be classified in 4 groups: (i) collapsed spindles, characterized by very robust asters but a decrease in spindle fibers, as well as shorter distances between centrosomes; (ii) weak spindles, characterized by the absence of spindle fibers; as well as (iii) monopolar or (iv)

Figure 4. Genetic ablation of Tpx2 causes a spindle assembly checkpoint-dependent delay in mitotic exit. **A**, time-lapse imaging of wild-type and Tpx2 null cells expressing H2B fused to mRFP. Images were taken every 10 minutes. Bars represent the fate of individual cells in the right panel. Ninety-seven percent of Tpx2 null cells ($N = 34$) carried out aberrant mitosis without chromosome segregation. Scale bar, 20 μm . **B**, length of mitosis was quantified in cells treated or not treated with siRNAs against Mad2 in the presence and the absence of nocodazole (Noc). The delay in mitotic exit was rescued by abrogation of Mad2 (22–25 cells were scored in each condition; ***, $P < 0.0001$). Right panel shows Mad2 protein levels in control and experimental cells transfected with scramble (Scr.) or Mad2-specific siRNAs (siMad2; ***, $P < 0.0001$). **C**, fate of $Tpx2^{\text{lox/lox}}$ and $Tpx2^{\Delta/\Delta}$ individual cells in the previous experiment.



multipolar spindles (Fig. 5A). To test whether multipolar spindles were a consequence of overnumerous centrosomes, we used the centriolar marker Cep135, a protein essential for centriole biogenesis (23, 24). Only 2 of the microtubule organizer centers were positive for Cep135 in these abnormal cells (Fig. 5A), although all of them were positive for γ -tubulin (data not shown), confirming that the phenotype was not a result of overnumerous centrosomes. Total α -tubulin intensity was normal in the aberrant spindles suggesting that microtubule formation itself, and not levels of α -tubulin, was altered in Tpx2 null cells (Supplementary Fig. S2).

Tpx2 interacts with several molecules, including the kinase Aurora A (6–8), the microtubule-sliding kinesin Eg5 (25, 26), and the plus-end directed kinesin Hklp2/Kif15 (2, 27). We therefore analyzed the status of these proteins in Tpx2-depleted cells. Although Aurora A was not totally displaced from the spindle, we found a significant reduction in the levels of the kinase at spindle microtubules ($P < 0.0001$; Fig. 5B). In agreement with data previously reported by 2 different groups (27, 28), the spindle localization of Kif15 was dramatically impaired in the absence of Tpx2 ($P < 0.0001$; Fig. 5B). Finally, we found no alterations in centrosome or microtubule

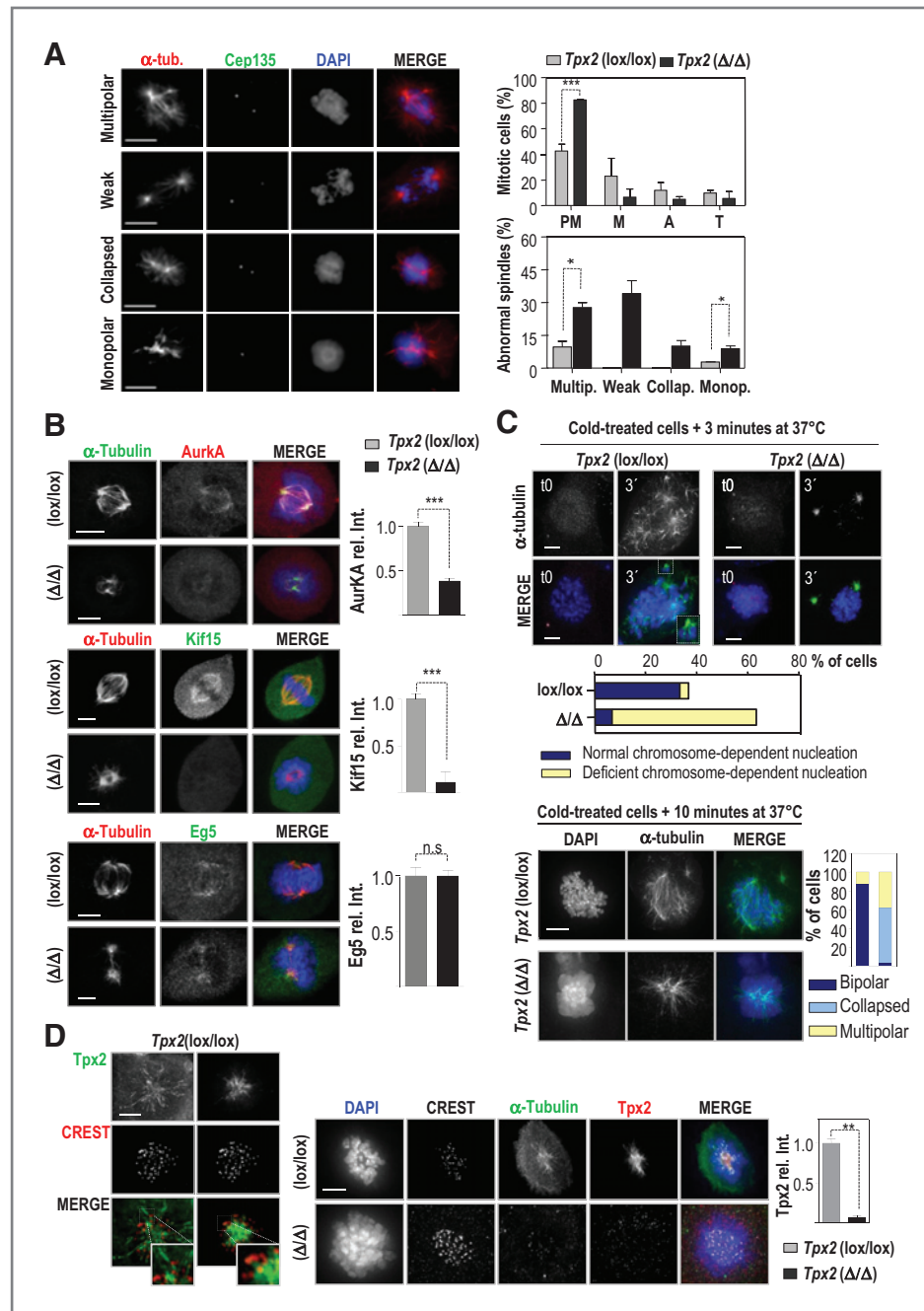


Figure 5. Defective microtubule nucleation in $Tpx2$ null cells. **A**, representative images of the spindle abnormalities displayed in $Tpx2^{\Delta/\Delta}$ cells are shown in the left panels. DAPI was used to stain the DNA, α -tubulin to label the microtubules in red, and Cep135 the centrosome in green. Scale bar, 5 μ m. The top histogram shows the distribution of mitotic phases as determined by immunofluorescence. Notice the significant (***) increase in prometaphase figures. Bottom histogram panel shows the distribution of mitotic aberrations in $Tpx2^{lox/lox}$ and $Tpx2^{\Delta/\Delta}$ (*, $P < 0.05$). **B**, localization of Aurora A (red), Kif15, and Eg5 (both in green) in $Tpx2$ null cells. Scale bars, 5 μ m. The fluorescence intensity of Aurora A Kif15 and Eg5 is represented in the histograms (**, $P < 0.0001$; n.s., $P = 1$). **C**, deficient chromatin-dependent microtubule nucleation in $Tpx2$ null cells 3 minutes (top) after cold treatment. α -Tubulin signals (green) in the vicinity of the chromosomes (DAPI in blue) were used as a marker of chromatin-driven nucleation. In addition, cells were incubated at 37°C during 10 minutes after cold treatment to allow further spindle formation. Quantification of spindle abnormalities is shown in the lower graph. Note that $Tpx2^{\Delta/\Delta}$ cells were unable to establish robust bipolar spindles after cold treatment. Scale bars, 5 μ m. **D**, $Tpx2^{lox/lox}$ MEFs were incubated on ice for 5 minutes to depolymerize nonstable microtubules (left). The specific localization of Tpx2 at k-fibers was confirmed by kinetochore staining with CREST (red) and anti-Tpx2 antibody (green; left). The stability of $Tpx2^{\Delta/\Delta}$ k-fibers is defective in the absence of Tpx2 (red; right) as detected by α -tubulin staining (green). CREST is in white and DAPI in blue. Scale bars, 5 μ m. The quantification of Tpx2 fluorescence intensity is shown in the right plot (**, $P < 0.01$).

localization of Eg5 in the aberrant spindles of $Tpx2^{\Delta/\Delta}$ cells (Fig. 5B).

We then analyzed microtubule dynamics by carrying out microtubule repolymerization assays. We ablated Tpx2 expression and promoted depolymerization of microtubules by keeping the culture on ice for 40 minutes following the protocol depicted in Fig. 3B. Repolymerization was analyzed after incubating the cells at 37°C for 3 minutes, to check microtubule nucleation from chromatin, or 10 minutes, to examine centrosome-dependent microtubule growth. As observed after knock down of TPX2 in human cell lines (3, 4), Tpx2 null MEFs presented a clear defect in α -tubulin polymerization from DNA. After 3 minutes at 37°C, short α -tubulin fibers coming from DNA were evident (green signal) in $Tpx2^{+/+}$ cells whereas $Tpx2^{\Delta/\Delta}$ MEFs presented a severe decrease in microtubule formation from chromatin (Fig. 5C). Note that nucleation from centrosomes was not affected as fibers were normally formed from centrosomes. Importantly, spindles in $Tpx2^{\Delta/\Delta}$ MEFs were abnormal after 10 minutes at 37°C, being collapsed or multipolar in 59% and 38% of cases, respectively (Fig. 5C). All these results showed that lack of Tpx2 leads to defective microtubule polymerization from the chromatin resulting in aberrant spindle formation.

The specific localization of Tpx2 and its implication in the stability of k-fibers prompted us to analyze the status of those fibers in $Tpx2^{\Delta/\Delta}$ MEFs. When cells are given cold treatment for short periods of time, the less stable microtubules are depolymerized initially, leaving intact the more stable k-fibers. When the cold treatment is maintained for longer periods, the stability of those k-fibers is also compromised. We treated $Tpx2^{lox/lox}$ and $Tpx2^{\Delta/\Delta}$ cells with the kinesin Eg-5 inhibitor monastrol to induce monopolar spindle formation and easily visualize the fibers in the spindles. Tpx2 was specifically localized to k-fibers (Fig. 5D, left panels). By increasing the cold treatment up to 5 minutes, k-fibers were totally lost in $Tpx2^{\Delta/\Delta}$ but not control cells ($P = 0.0034$; Fig. 5D, right panels), indicating that Tpx2 confers stability to k-fibers possibly facilitating chromosome capture. All these data point out the relevance of Tpx2 in the initial steps of spindle formation and also in the stabilization of the bipolar required for accurate chromosome segregation.

Increased aneuploidy and tumor formation in the presence of abnormal Tpx2 levels

Given the requirements for Tpx2 in spindle integrity and genomic stability, we wondered whether Tpx2 haploinsufficiency could lead to accumulation of aneuploidy. $Tpx2^{+/-}$ mice display a general reduction in Tpx2 mRNA levels both in proliferative (testis, skin, and intestine) and nonproliferative (kidney, brain, and liver) tissues (Supplementary Fig. S3). We extracted splenocytes from $Tpx2^{+/-}$ mice, stimulated them with mitogens, and carried out karyotype analysis. Sixteen-week-old $Tpx2^{+/-}$ mice presented higher grade of aneuploidy and 18.3% of cells showed karyotypes that varied from 35 to 80 chromosomes per cell whereas control littermate mice were always 40 or 41 chromosomes per metaphase (Fig. 6A). These control mice always kept 39 to 41 chromosomes even at 90

weeks of age. In contrast, the percentage of aneuploid cells increased to 27% in old $Tpx2^{+/-}$ mice. These data suggested that Tpx2 plays a critical role in maintaining cellular ploidy of mammals *in vivo*.

$Tpx2^{+/-}$ mice, albeit being healthy at birth and totally fertile, showed shorter tumor-free lifespan than their wild-type littermates (Fig. 6B). The histopathologic analysis of the 2 cohorts of $Tpx2^{+/+}$ ($n = 14$) and $Tpx2^{+/-}$ ($n = 17$) mice indicated increased development of spontaneous tumors in mutant mice (53% incidence in $Tpx2^{+/-}$ vs. 7.1% in wild-type mice; $P < 0.001$). The most common tumors developed by $Tpx2^{+/-}$ mice were lymphomas (35.3% of the tumors vs. 7.1% in wild-type mice; Fig. 6B). These mutant lymphomas were not only more abundant but also showed highest aggressiveness as shown by the infiltrations in brain, which are uncommon in other models, and heart among other tissues (Fig. 6C). $Tpx2^{+/-}$ tumors presented higher levels of aneuploidy (48.9% of aneuploid cells) when compared with $Tpx2^{+/-}$ healthy tissues or wild-type control splenocytes (Fig. 6C).

$Tpx2^{+/-}$ mice also developed frequent lung tumors (alveolar type II cell adenomas and adenocarcinomas; 29.4%; Fig. 6D), as well as other pathologies that were not observed in the wild-type controls, including hyperplasia in the pars intermedia of the pituitary (11.8%; Fig. 6D). All these results indicated that an abnormal expression of Tpx2 can favor tumor development *in vivo*.

Discussion

We report in this article that lack of Tpx2 causes early embryonic lethality during preimplantational development in the mouse. Tpx2 null embryos fail to form blastocysts due to the formation of collapsed spindles and lack of chromosome segregation. Genetic ablation of Eg-5 (kinesin-5), a plus-end-directed motor involved in bipolar spindle formation and maintenance during mitosis, is also associated with early embryonic lethality mainly due to the accumulation of monopolar cells arrested in prometaphase that collapse and are not able to progress beyond the blastocyst stage (29, 30). Interestingly, embryos deficient for Aurora A, probably the main mitotic kinase involved in spindle formation, are also arrested at the same early stages of development (15, 31, 32). Thus, the lack of proteins with major functions in spindle formation and maintenance seems to prevent embryonic development at very early stages.

Tpx2-deficient MEFs require more time than control cells to enter into mitosis (not shown), transiently arrest at prometaphase, and finally exit mitosis without dividing in 2 daughter cells. All these features are also found in Aurora A null primary MEFs (15, 31, 32), which is consistent with the role of Tpx2 as a critical regulator of the Aurora A kinase (4, 6, 8, 33–35). However, some differences are detected between these 2 models suggesting separate functions. For instance, conditional genetic ablation of Tpx2, but not Aurora A, results in a significant induction of apoptosis in primary MEFs. In addition, whereas monopolar spindles are rare in Tpx2 null cells, these figures are frequently observed in Aurora A-deficient fibroblasts MEFs (15, 31, 32), suggesting that this kinase plays a

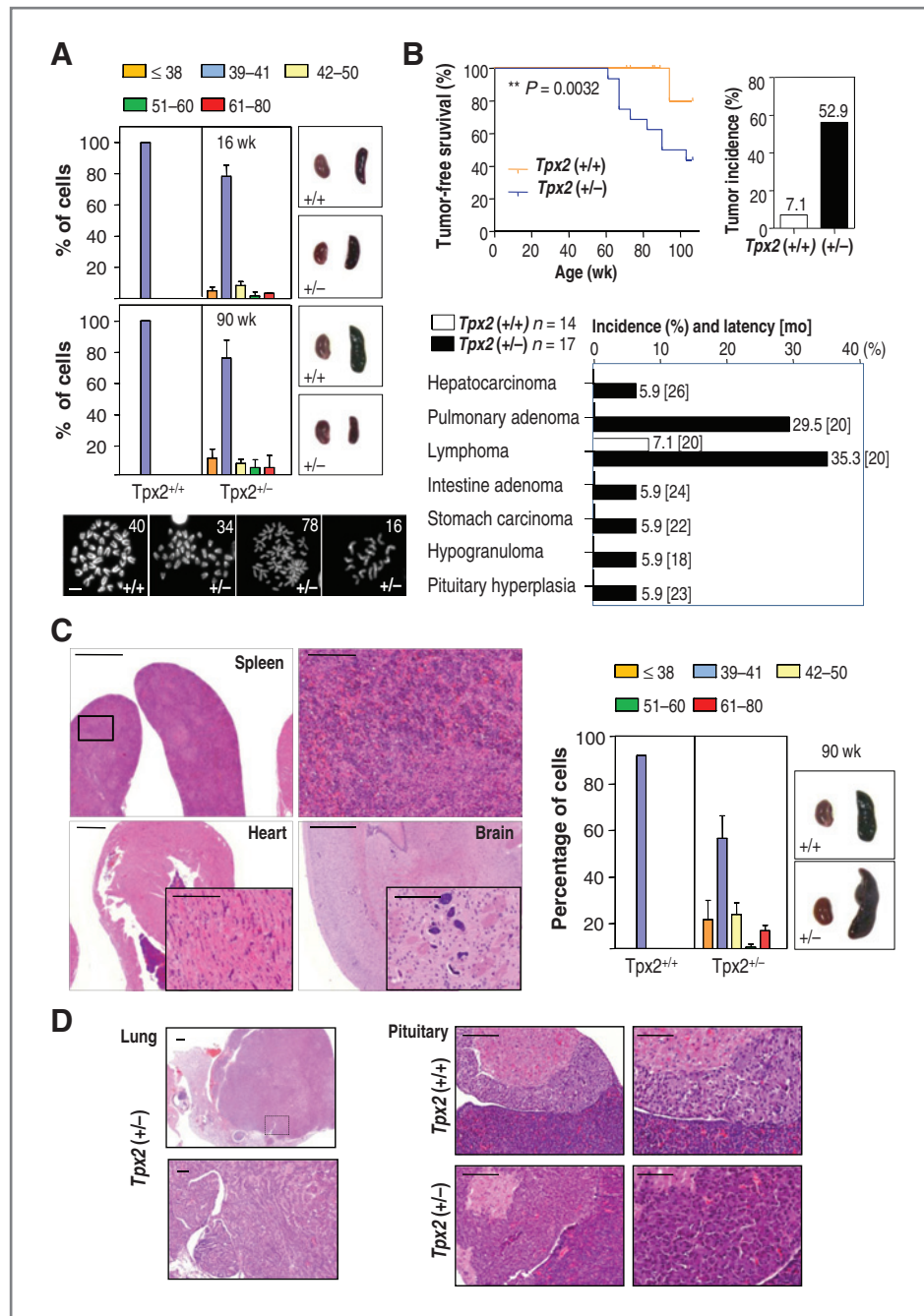


Figure 6. *Tpx2* heterozygous mice accumulate aneuploid cells and are prone to develop spontaneous lymphomas and adenocarcinomas. **A**, splenocytes were harvested from *Tpx2*^{+/+} and *Tpx2*^{+/-} mice and kept in culture for 72 hours in the presence of lipopolysaccharide to promote proliferation. *Tpx2*^{+/+} mice retain euploid karyotypes whereas *Tpx2*^{+/-} accumulate aberrations in chromosome inheritance. Chromosomes from 30 cells were counted in each plate. Scale bar, 5 μ m. Representative pictures of spleens are shown. Kidney is used as a reference for size. **B**, tumor-free survival of *Tpx2*^{+/+} ($N = 14$) and *Tpx2*^{+/-} ($N = 17$) mice, showing a statistically significant shortening in *Tpx2*^{+/-} life span ($P = 0.0032$). The incidence of tumors and the type of pathologies found in these mice is also shown. **C**, spleen lymphomas in *Tpx2*^{+/-} mice are characterized by their high-grade aggressiveness including spreading to the heart and brain (H&E staining). Scale bars, 1,000 μ m or 200 μ m (top right and insets). The ploidy of tumor cells from the spleen in *Tpx2*^{+/-} mice is also shown and compared with normal, 90-week old splenocytes from wild-type mice. **D**, representative lung alveolar type II adenocarcinoma [left; scale bars, 500 μ m (top) and 200 μ m (bottom)] and hyperplasia in pars intermedia of the pituitary gland in *Tpx2*^{+/-} mice, compared with normal pituitary in control animals [right; scale bars, 200 μ m (left) or 100 μ m (right)].

major role in centrosome maturation and separation in a *Tpx2*-independent manner.

Tpx2 is known to regulate the formation of the spindle by promoting microtubule nucleation from the chromatin and stabilizing the spindle microtubules in a Ran-dependent manner (3, 5, 36). In *Tpx2* null MEFs, chromosome capture by astral microtubules seems normal. However *Tpx2* ^{Δ/Δ} mitotic cells are defective in tubulin polymerization from chromatin, which would result in the lack of antiparallel spindle fibers and eventually in the establishment of a weak bipolar spindle. The structural problems displayed by *Tpx2* null spindles may result,

at least in part, from the absence of essential forces exerted by kinesins such as Eg-5 or Kif15 that ensure spindle elongation. The lack of Kif15 localization in *Tpx2* knocked down cells (27) favors this hypothesis. Similarly, the normal microtubule associated localization of Aurora A is lost in *Tpx2* null cells (6). The relative contribution of these defects to the phenotype observed in the absence of *Tpx2* remains elusive, given the technical difficulties of restoring the localization of these proteins in *Tpx2* null cells.

Tpx2 is overexpressed in several tumor types such as cervical, lung, and ovarian carcinoma as well as in giant-

cell tumors of bone, where it is amplified (37–40). Moreover, Tpx2 overexpression correlates positively with tumor grade and stage, presence of lymphometastasis, and bad prognosis (41–43). Furthermore, Tpx2 displays the highest correlation with chromosome instability (CIN) among a signature of genes deregulated in human tumors (17). Here, we have shown that genetic ablation of Tpx2 results in chromosome segregation defects and the generation of tetraploid or aneuploid cells. *Tpx2*^{+/-} mice are also prone to develop a wide spectrum of tumor types, suggesting that this protein may function as a tumor suppressor protecting from genomic instability. A similar increase in the development of spontaneous tumors has been observed in haploinsufficient mouse models of other mitotic genes, including Aurora A, CenpE, Mad2, or Cdh1 (11). All together, the fact that overexpression of some of these proteins such as Aurora A, Mad2, or Tpx2 also promotes tumor development in mouse models or correlated with tumor development in human malignancies favor the idea that subtle changes, either up or down, in the level of expression of the same mitotic regulator might have important consequences in genomic instability and cancer development. *Tpx2*^{+/-} mice accumulate aneuploidy with age indicating that their tissues are genetically unstable. This feature correlates with

increased susceptibility to tumor development, supporting the idea that Tpx2 deregulation might eventually act as a driving force of tumor development by the induction of aneuploidy.

Disclosure of Potential Conflicts of Interest

No potential conflicts of interest were disclosed.

Acknowledgments

The authors thank Susana Temiño and Beatriz Escobar for technical assistance, and Y. Arlot-Bonnemains (CNRS, Université de Rennes, Rennes) and Isabelle Vernos (Centro for Genomic Research, Barcelona) for reagents.

Grant Support

This work was funded by grants from the Association for International Cancer Research (AICR #08-0188), Foundation Ramón Areces, and the Spanish Ministry of Science and Innovation (MICINN; SAF2010-19710 to I.P. de Castro and SAF2009-07973 to M. Malumbres). The Cell Division and Cancer Group of the CNIO is supported by the OncoCycle Programme (S-BIO-0283-2006) from the Comunidad de Madrid, the OncoBIO Consolider-Ingenio 2010 Programme (CSD2007-00017) from the MICINN, Madrid. A. Hyman and M. Malumbres laboratories are supported by the European Union Seventh Framework Programme (MitoSys project; HEALTH-F5-2010-241548).

The costs of publication of this article were defrayed in part by the payment of page charges. This article must therefore be hereby marked *advertisement* in accordance with 18 U.S.C. Section 1734 solely to indicate this fact.

Received June 10, 2011; revised December 28, 2011; accepted January 14, 2012; published OnlineFirst January 20, 2012.

References

- Kalab P, Pralle A, Isacoff EY, Heald R, Weis K. Analysis of a RanGTP-regulated gradient in mitotic somatic cells. *Nature* 2006;440:697–701.
- Wittmann T, Boleti H, Antony C, Karsenti E, Vernos I. Localization of the kinesin-like protein Xklp2 to spindle poles requires a leucine zipper, a microtubule-associated protein, and dynein. *J Cell Biol* 1998;143:673–85.
- Tulu US, Fagerstrom C, Ferenz NP, Wadsworth P. Molecular requirements for kinetochore-associated microtubule formation in mammalian cells. *Curr Biol* 2006;16:536–41.
- Bird AW, Hyman AA. Building a spindle of the correct length in human cells requires the interaction between TPX2 and Aurora A. *J Cell Biol* 2008;182:289–300.
- Gruss OJ, Carazo-Salas RE, Schatz CA, Guarguaglini G, Kast J, Wilm M, et al. Ran induces spindle assembly by reversing the inhibitory effect of importin alpha on TPX2 activity. *Cell* 2001;104:83–93.
- Kufer TA, Sillje HH, Komer R, Gruss OJ, Meraldi P, Nigg EA. Human TPX2 is required for targeting Aurora-A kinase to the spindle. *J Cell Biol* 2002;158:617–23.
- Eyers PA, Erikson E, Chen LG, Maller JL. A novel mechanism for activation of the protein kinase Aurora A. *Curr Biol* 2003;13:691–7.
- Tsai MY, Wiese C, Cao K, Martin O, Donovan P, Ruderman J, et al. A Ran signalling pathway mediated by the mitotic kinase Aurora A in spindle assembly. *Nat Cell Biol* 2003;5:242–8.
- Bayliss R, Sardon T, Vernos I, Conti E. Structural basis of Aurora-A activation by TPX2 at the mitotic spindle. *Mol Cell* 2003;12:851–62.
- Perez de Castro I, de Carcer G, Malumbres M. A census of mitotic cancer genes: new insights into tumor cell biology and cancer therapy. *Carcinogenesis* 2007;28:899–912.
- Schvartzman JM, Sotillo R, Benezra R. Mitotic chromosomal instability and cancer: mouse modelling of the human disease. *Nat Rev Cancer* 2010;10:102–15.
- Holland AJ, Cleveland DW. Boveri revisited: chromosomal instability, aneuploidy and tumorigenesis. *Nat Rev Mol Cell Biol* 2009;10:478–87.
- Michel LS, Liberal V, Chatterjee A, Kirchwegger R, Pasche B, Gerald W, et al. MAD2 haplo-insufficiency causes premature anaphase and chromosome instability in mammalian cells. *Nature* 2001;409:355–9.
- Sotillo R, Hernando E, Diaz-Rodriguez E, Teruya-Feldstein J, Cordon-Cardo C, Lowe SW, et al. Mad2 overexpression promotes aneuploidy and tumorigenesis in mice. *Cancer Cell* 2007;11:9–23.
- Lu LY, Wood JL, Ye L, Minter-Dykhouse K, Saunders TL, Yu X, et al. Aurora A is essential for early embryonic development and tumor suppression. *J Biol Chem* 2008;283:31785–90.
- Asteriti IA, Rensen WM, Lindon C, Lavia P, Guarguaglini G. The AuroraA/TPX2 complex: a novel oncogenic holoenzyme? *Biochim Biophys Acta* 2010;1806:230–9.
- Carter SL, Eklund AC, Kohane IS, Harris LN, Szallasi Z. A signature of chromosomal instability inferred from gene expression profiles predicts clinical outcome in multiple human cancers. *Nat Genet* 2006;38:1043–8.
- Malumbres M, Mangués R, Ferrer N, Lu S, Pellicer A. Isolation of high molecular weight DNA for reliable genotyping of transgenic mice. *Biotechniques* 1997;22:1114–9.
- García-Higuera I, Manchado E, Dubus P, Canamero M, Mendez J, Moreno S, et al. Genomic stability and tumour suppression by the APC/C cofactor Cdh1. *Nat Cell Biol* 2008;10:802–11.
- Kanda T, Sullivan KF, Wahl GM. Histone-GFP fusion protein enables sensitive analysis of chromosome dynamics in living mammalian cells. *Curr Biol* 1998;8:377–85.
- Schnutgen F, De-Zolt S, Van Sloun P, Hollatz M, Floss T, Hansen J, et al. Genomewide production of multipurpose alleles for the functional analysis of the mouse genome. *Proc Natl Acad Sci U S A* 2005;102:7221–6.
- Musacchio A, Salmon ED. The spindle-assembly checkpoint in space and time. *Nat Rev Mol Cell Biol* 2007;8:379–93.
- Ohta T, Essner R, Ryu JH, Palazzo RE, Uetake Y, Kuriyama R. Characterization of Cep135, a novel coiled-coil centrosomal protein involved in microtubule organization in mammalian cells. *J Cell Biol* 2002;156:87–99.
- Kleylein-Sohn J, Westendorf J, Le Clech M, Habedanck R, Stierhof YD, Nigg EA. Plk4-induced centriole biogenesis in human cells. *Dev Cell* 2007;13:190–202.
- Ma N, Tulu US, Ferenz NP, Fagerstrom C, Wilde A, Wadsworth P. Poleward transport of TPX2 in the mammalian mitotic spindle requires dynein, Eg5, and microtubule flux. *Mol Biol Cell* 2010;21:979–88.

26. Ma N, Titus J, Gable A, Ross JL, Wadsworth P. TPX2 regulates the localization and activity of Eg5 in the mammalian mitotic spindle. *J Cell Biol* 2011;195:87–98.
27. Vanneste D, Takagi M, Imamoto N, Vernos I. The role of Hk1p2 in the stabilization and maintenance of spindle bipolarity. *Curr Biol* 2009;19:1712–7.
28. Tanenbaum ME, Macurek L, Janssen A, Geers EF, Alvarez-Fernandez M, Medema RH. Kif15 cooperates with eg5 to promote bipolar spindle assembly. *Curr Biol* 2009;19:1703–11.
29. Castillo A, Justice MJ. The kinesin related motor protein, Eg5, is essential for maintenance of pre-implantation embryogenesis. *Biochem Biophys Res Commun* 2007;357:694–9.
30. Chauviere M, Kress C, Kress M. Disruption of the mitotic kinesin Eg5 gene (*Knsl1*) results in early embryonic lethality. *Biochem Biophys Res Commun* 2008;372:513–9.
31. Cowley DO, Rivera-Perez JA, Schliekelman M, He YJ, Oliver TG, Lu L, et al. Aurora-A kinase is essential for bipolar spindle formation and early development. *Mol Cell Biol* 2009;29:1059–71.
32. Sasai K, Parant JM, Brandt ME, Carter J, Adams HP, Stass SA, et al. Targeted disruption of Aurora A causes abnormal mitotic spindle assembly, chromosome misalignment and embryonic lethality. *Oncogene* 2008;27:4122–7.
33. Eyers PA, Maller JL. Regulation of *Xenopus* Aurora A activation by TPX2. *J Biol Chem* 2004;279:9008–15.
34. Tsai MY, Zheng Y. Aurora A kinase-coated beads function as microtubule-organizing centers and enhance RanGTP-induced spindle assembly. *Curr Biol* 2005;15:2156–63.
35. Giubettini M, Asteriti IA, Scrofani J, De Luca M, Lindon C, Lavia P, et al. Control of Aurora-A stability through interaction with TPX2. *J Cell Sci* 2010;124:113–22.
36. Trieselmann N, Armstrong S, Rauw J, Wilde A. Ran modulates spindle assembly by regulating a subset of TPX2 and Kid activities including Aurora A activation. *J Cell Sci* 2003;116:4791–8.
37. Ramakrishna M, Williams LH, Boyle SE, Bearfoot JL, Sridhar A, Speed TP, et al. Identification of candidate growth promoting genes in ovarian cancer through integrated copy number and expression analysis. *PLoS One* 2010;5:e9983.
38. Scotto L, Narayan G, Nandula SV, Arias-Pulido H, Subramaniyam S, Schneider A, et al. Identification of copy number gain and overexpressed genes on chromosome arm 20q by an integrative genomic approach in cervical cancer: potential role in progression. *Genes Chromosomes Cancer* 2008;47:755–65.
39. Smith LT, Mayerson J, Nowak NJ, Suster D, Mohammed N, Long S, et al. 20q11.1 amplification in giant-cell tumor of bone: Array CGH, FISH, and association with outcome. *Genes Chromosomes Cancer* 2006;45:957–66.
40. Tonon G, Wong KK, Maulik G, Brennan C, Feng B, Zhang Y, et al. High-resolution genomic profiles of human lung cancer. *Proc Natl Acad Sci U S A* 2005;102:9625–30.
41. Ma Y, Lin D, Sun W, Xiao T, Yuan J, Han N, et al. Expression of targeting protein for *xk1p2* associated with both malignant transformation of respiratory epithelium and progression of squamous cell lung cancer. *Clin Cancer Res* 2006;12:1121–7.
42. Shigeishi H, Ohta K, Hiraoka M, Fujimoto S, Minami M, Higashikawa K, et al. Expression of TPX2 in salivary gland carcinomas. *Oncol Rep* 2009;21:341–4.
43. Li B, Qi XQ, Chen X, Huang X, Liu GY, Chen HR, et al. Expression of targeting protein for *Xenopus* kinesin-like protein 2 is associated with progression of human malignant astrocytoma. *Brain Res* 2010;1352:200–7.